Proceedings of ASME Turbo Expo 2011
GT2011
June 6-10, 2011, Vancouver, British Columbia, Canada

GT2011-45376

EXPERIMENTAL INVESTIGATION INTO THE IMPACT OF CROSSFLOW ON THE COHERENT UNSTEADINESS WITHIN FILM COOLING FLOWS

Richard J. Fawcett
Department of Engineering Science
University of Oxford
United Kingdom
richard.fawcett@eng.ox.ac.uk

Andrew P S Wheeler
School of Engineering and Materials Science
Queen Mary, University of London
United Kingdom

Li He
Department of Engineering Science
University of Oxford
United Kingdom

Rupert Taylor
Rolls-Royce
Turbine Systems, Bristol
United Kingdom

ABSTRACT

It is known that the mixing of a film cooling flow with the main turbine passage flow is an unsteady process, with coherent unsteady features occurring across a range of blowing ratios. Upon an aero engine the cooling holes on a turbine blade commonly have a crossflow at the hole inlet. Previous work has shown that crossflow at the hole inlet modifies the time-mean flowfield downstream of a cooling hole compared to the case without crossflow.

The current paper investigates the impact of spanwise orientated crossflow on the coherent unsteadiness within film cooling flows. Both cylindrical and fan-shaped holes, located on a blade pressure surface, are studied. The range of blowing ratios considered is 0.7 to 1.8 and the crossflow velocity is up to 0.8 times the bulk jet velocity. High Speed Photography and Hot Wire Anemometry are used to observe the presence of coherent unsteadiness, both immediately downstream of the hole exit and within the cooling hole tube.

The results show that the coherent unsteadiness downstream of the hole exit is persistent and its occurrence is not significantly affected by the magnitude of spanwise crossflow. Within the cooling hole tube the existence of coherent unsteadiness is presented for the first time, inside both cylindrical and fan-shaped holes, with a Strouhal number of 0.6 to 0.8. The pattern of this in-hole coherent unsteadiness is seen to change with increasing the crossflow velocity.

NOMENCLATURE

A Area
C_p Pressure Coefficient
D Hole Diameter
f Frequency
M Blowing Ratio
$\dot{m}$ Mass Flow Rate
CFR Crossflow to Bulk Jet Velocity Ratio
p Pressure
V Velocity
ρ Density

Subscripts

c Coolant, Cooling Holes
$cross$ Crossflow Channel
e Exit
in Plenum In

Copyright © 2011 by Rolls-Royce plc

out Crossflow Channel Overflow
∞ Hole exit
01 Inlet Total

INTRODUCTION

The efficiency of an aero engine has been increased significantly by raising the temperature at the turbine inlet. Film cooling has been used since the 1960s [1] to cool the surface of turbine blades and vanes to withstand these higher temperatures. The coolant used in film cooling must be drawn from the compressor, so its use decreases the engine core thermal efficiency. Whilst the mixing between the coolant and the main turbine passage flow will lead to a reduction in the turbine stage efficiency. Consequently film cooling flows are designed to maximise film effectiveness, whilst minimising the quantity of coolant used.

Previous experimental research into film cooling flows has predominantly focused on time-averaged surface measurements of the film effectiveness downstream of the cooling hole exit, for example those of Goldstein et al [2] and Sinha et al [3]. Only a few studies, including those of Pietrzyk et al [4] and Thole et al [5], have presented the time-mean aerodynamic flowfield downstream of a cooling hole.

The experimental results presented by Andreopoulos [6], Fric and Roshko [7], Kelso et al [8] and Lim et al [9] for a jet entering normal to an external crossflow have shown that the mixing between the two is an unsteady process, with coherent unsteadiness present within the shear layer. Matsuda et al [10] have shown the occurrence of coherent hairpin vortices of a Strouhal number of 0.5 within a wall jet.

For hole geometries typical of film cooling, Tyagi and Achraya [11] have shown computationally for a cylindrical hole with a blowing ratio equal to 1.0 the existence of hairpin vortices of a Strouhal number equal to 1.0. The experiments of Fawcett et al [12] show the existence of shear layer vortices within the jet from a cylindrical hole of a blowing ratio of 2.0, and hairpin vortices in the jet from a fan-shaped hole of blowing ratio equal to 0.5.

Most film cooling investigations have had their cooling holes fed from a plenum chamber. Cooling holes are typically fed from a serpentine passage running spanwise within the blade interior, thus meaning that a crossflow is present at the hole inlet. A series of studies into the effect of internal crossflow on film cooling effectiveness have been undertaken at the Universität Karlsruhe [13], [14] and [15], for cylindrical and fan-shaped holes. Three crossflow configurations were considered, ‘co-flow’,‘counter’ and ‘spanwise’. Changes in the film effectiveness downstream suggest that the presence of spanwise crossflow is advantageous to a cylindrical hole, but is detrimental to the performance of a fan-shaped hole [15].

The cooling hole tube links the crossflow passage to the downstream flowfield. Peterson and Plesniak [16] and Thole et al [17] have showed experimentally, and Kohli and Thole [18] computationally, that changing the crossflow direction changes the time-mean flowfield inside the cooling hole tube.

Crossflow at the hole inlet is known to impact upon the time-mean flowfield. The current study questions whether this change is due to changes in the coherent unsteady structures which are present in film cooling flows. The investigation looks at both the flowfield downstream of the cooling hole exit and that inside the cooling hole tube. Cylindrical and fan-shaped holes, located within a row of holes upon the pressure surface of a engine representative turbine blade, are investigated. A blowing ratio range of 0.7 to 1.8 is tested with an internal crossflow varying up to 0.8 times the bulk jet velocity.

High Speed Photography and Hot Wire Anemometry are used to sample the flowfield downstream of the cooling hole exit at up to 3kHz. Hot Wire Anemometry is also used to investigate the presence of coherent unsteadiness inside the cooling hole tube. The results show the existence of coherent hairpin vortices, vortices in the shear layer and coherent unsteadiness within the cooling hole tube. Within this paper the formation mechanisms are discussed, and how the picture is changed by varying the crossflow velocity. Coherent unsteadiness is seen at blowing ratios typical of film cooling, and therefore the conclusions presented here could have implications for the film cooling designer.

EXPERIMENTAL SETUP

Linear Cascade and Cooling Hole Geometry

The Oxford Super Scale cascade at the University of Oxford’s Southwell (Osney) laboratory was used for this investigation, (Palafox [19]). A plan view of the facility is shown in Fig 1. The flow enters through a bellmouth intake and first passes through a series of screens and flow straighteners. The flow then reaches the three passage linear cascade featuring low speed RT27a blades which have a true chord and span equal to 1m. The RT27a blade is able to replicate the C_p distribution of a high pressure turbine blade in a low pressure environment. The C_p profile for the blade is also shown in Fig. 1. At the exit of the cascade the flow passes into a 4m by 2m wind tunnel.

The Reynolds number for the current experiments, based on the true chord and the cascade exit velocity, was 6×10^5. The turbulence intensity of the flow entering the cascade was 2% measured on a plane 1.6m upstream of the blade leading edge. It is likely that this turbulence intensity is lower than the value upstream of a High Pressure Turbine blade.

It has been detailed by Fawcett et al [12] that the Oxford Super Scale cascade has been modified to include a row of five cooling holes on the blade pressure surface at 50% axial chord. At this location the boundary layer has a shape factor of 1.9. Within this previous work the cylindrical and fan-shaped cooling holes were fed from a plenum chamber inside the blade interior.

 Copyright © 2011 by Rolls-Royce plc

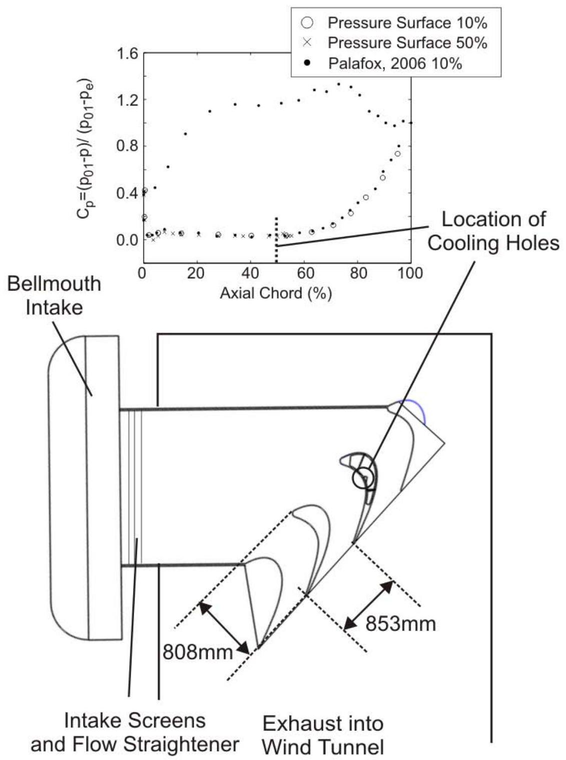

Figure 1. Plan view of the Oxford Super Scale Cascade, and the blade C_p profile.

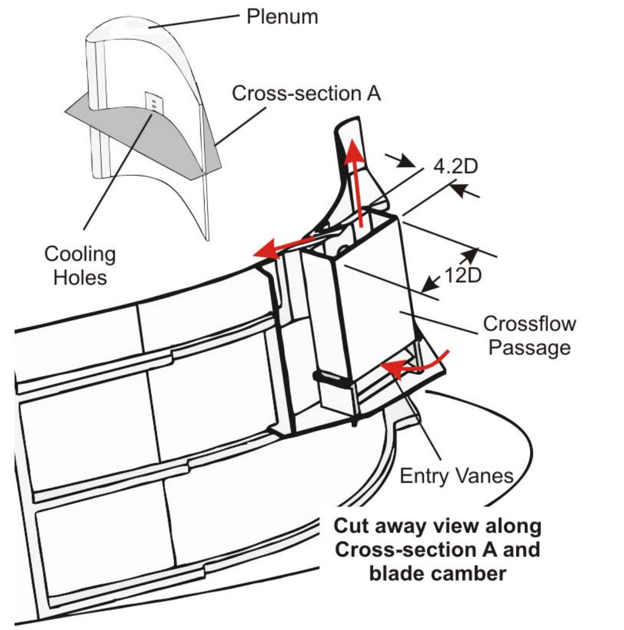

Figure 2. Cut away view of the blade interior to show the crossflow channel located inside the plenum chamber.

For the current experiment the blade interior was modified so that the cooling holes were fed by a crossflow channel orientated in the spanwise direction. Figure 2 shows a cutaway view of the crossflow passage located within the plenum chamber.

A 690kPa (100psi) high pressure air line was used to supply coolant and crossflow into the plenum. The coolant entered the plenum through the upper wall, from a pipe of 59mm diameter with a bellmouth exit. The coolant entered the crossflow passage at the bottom of the plenum. Curved entry vanes were used at the entrance to the crossflow channel to minimise the losses and non-uniformities caused by turning the coolant through 90°. The crossflow channel had a width of 12D (hole diameters) and a height of 4.2D, with the cooling hole inlet being located midway across the channel width. The centre cooling hole was 18D downstream of the crossflow channel entrance.

The coolant in the crossflow channel that did not exit through the cooling holes was drawn into a pipe 18D downstream of the centre cooling hole. This pipe delivered the excess coolant to a blower, where the necessary pressure rise was supplied so that it could be exhausted into the wind tunnel downstream of the cascade.

Cylindrical and fan-shaped cooling holes were investigated in the current study. The rows of five cooling holes were manufactured upon a removable module made using a stereolithography technique. The results presented in the next chapter are all based on the centre hole, located on the blade mid span. The geometries of the cooling holes are shown in Fig. 3, and except for the hole inlet the dimensions are identical to those described in Fawcett et al [12].

The cooling hole diameter (D) was 12mm and was chosen so as to have a ratio with respect to the blade chord typical of a high pressure turbine blade. The hole length was 6D and the pitch spacing was 3D. The axis of the cooling hole was orientated at an angle of 30° to the sidewall of the crossflow channel and 30° to a plane tangent to the blade surface at 50% axial chord. The fan-shaped hole featured a fan angle of 14° which started 3D from the hole exit centre and a laidback angle of 7° which began 1D upstream of the hole exit centre.

The mass flow rates into the plenum and through the outlet pipe from the crossflow passage were adjusted using valves. This allowed the blowing ratio (M) of the cooling holes and the ratio of crossflow velocity to the bulk jet velocity (CFR) to be varied. The mass flow rates through both the inlet and outlet pipes were

Copyright © 2011 by Rolls-Royce plc

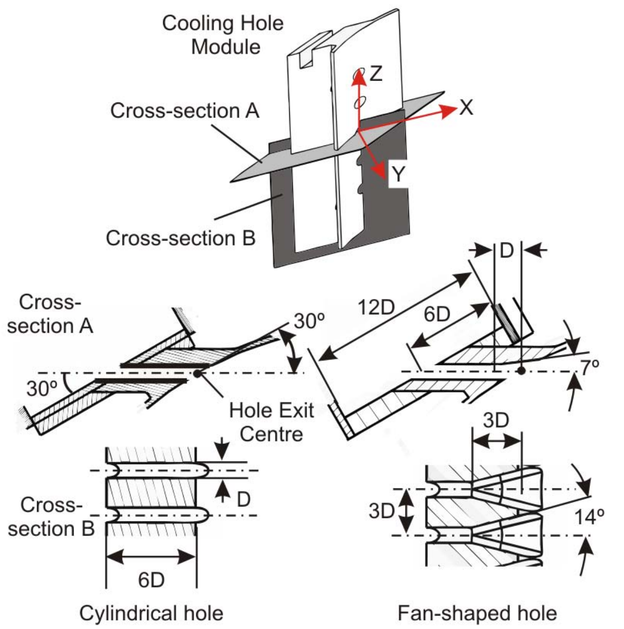

Figure 3. Cooling hole geometries: (top) interchangeable module, (lower-left) cylindrical hole and (lower-right) fan-shaped hole.

measured by means of orifice plates designed according to ISO standards [20]. The range of blowing ratios was 0.7 to 1.8, with crossflow velocities of up to 0.8 times the bulk jet velocity. The density ratio was unity and consequently the range of momentum ratio was 0.5 to 3.2. The corresponding range of hole Reynolds number, based on the hole diameter and jet bulk velocity, was 900 to 2300.

The blowing ratio (M) is calculated as the ratio of the coolant and mainstream mass fluxes according to Eq. 1. Here the coolant mass flux was obtained using the coolant mass flow rate ($\dot{m}_c$), and the throat area (A_c) of the five cooling holes. The coolant mass flow rate was found as the difference between the mass flow rate into the plenum ($\dot{m}_{in}$) and the mass flow rate out of the crossflow passage ($\dot{m}_{out}$). The inlet total pressure (p_{01}) was taken from a pitot probe located 1.6m upstream of the blade leading edge. The surface static pressure (p_∞) was the surface static pressure at 50% axial chord if there were no cooling holes. The surface static pressure (p_∞) was equivalent to the exit static pressure (p_e) found on the endwall of the cascade at mid-pitch multiplied by the appropriate blade C_p value found without cooling holes.

$$M = \frac{\rho_c V_c}{\rho_\infty V_\infty} = \frac{\dot{m}_c/A_c}{\sqrt{2\rho(p_{01}-p_\infty)}} = \frac{(\dot{m}_{in}-\dot{m}_{out})/A_c}{\sqrt{2\rho C_p(p_{01}-p_e)}} \quad (1)$$

The ratio of the crossflow velocity to the bulk jet velocity (CFR) was calculated according to Eq. 2. The crossflow velocity (V_{cross}) was the average velocity in the crossflow channel upstream of the cooling holes, and A_{cross} denotes the cross-sectional area of the crossflow channel. Within the results section a CFR of 0.1 refers to the minimum crossflow case where all of the coolant in the crossflow channel exits through the cooling holes.

$$CFR = \frac{V_{cross}}{V_c} = \frac{\dot{m}_{in}/\rho A_{cross}}{\dot{m}_{in}-\dot{m}_{out}/\rho A_c} = \frac{1}{1-\frac{\dot{m}_{out}}{\dot{m}_{in}}}\frac{A_c}{A_{cross}} \quad (2)$$

The low speed nature of the cascade (Mach No.$\sim$0.01) meant that the pressure difference measured to obtain the cascade dynamic pressure on the blade pressure surface was usually less than 10Pa. A Furness Controls FCO332 0-30Pa pressure transducer was selected to measure this small pressure differential.

In calculating the BR and CFR it was assumed that the coolant splits uniformly across the five cooling holes. As such the BR values quoted represent mean values across the row of holes. To confirm that the BR through the centre hole was consistent with this mean value, the velocity was measured at the hole exit centre using the Hot Wire Anemometry setup introduced in the following section. The BR based on this velocity and that in the mainstream was the same as the average value based on the mass flow rate.

Measurement Techniques

High Speed Photography and Hot Wire Anemometry were used to study the coherent unsteady features of the jet downstream of the cooling hole. Due to access restrictions only Hot Wire Anemometry was used inside the cooling hole.

The High Speed Photography was performed using a Photron APX camera capable of frame rates of up to 250kHz, with sheet illumination of the jet provided by an Oxford Lasers copper vapour laser capable of pulsing at up to 10kHz. The jet was seeded with smoke produced by a Concept Smoke Systems ViCount700 smoke machine, which fed into the pipe passing into the plenum chamber upstream of the orifice plate.

The camera and laser were orientated to observe the flowfield downstream of the centre cooling hole in two measurement planes, referred to within this paper as the spanwise and secondary flow planes. The spanwise plane was normal to the spanwise direction, with offsets relative to the blade midspan. The secondary flow plane was normal to the hole axis, with distances relative to the hole exit centre. Drawings are included on all the figures in the results chapter to show the orientation of the measurement plane with respect to the cooling hole.

The images shown in this paper were recorded with the camera and laser syncronised to record at 1kHz in the spanwise plane,

Copyright © 2011 by Rolls-Royce plc

and 1kHz or 3kHz in the secondary flow plane. Sequences 650 images in length were used to calculate the time-averaged flowfield and the frequency spectra.

The large size of the copper vapour laser meant that it had to be located away from the measurement area and the laser light delivered through a fibre optic cable. A disadvantage of this was that the method of creating the light sheet from the output of the fire optic cable created bands of low light intensity within the light sheet. These bands of low light intensity are apparent within the results section of this paper.

To minimise the impact of the variations in light sheet intensity, the mean intensity images shown in the results section were calculated based on the outcome of a detector function. This function first finds the maximum intensity over the entire recording for each point. For each frame if the intensity at a point was within 50% of the maximum intensity at that point the jet was classed as present, and a value of 1 assigned. If the intensity was less than 50% of the maximum then a value of 0 was assigned. To avoid generating noise in the regions where the jet was never present a lower limit was set for the maximum intensity.

To identify the passing frequencies of the unsteady structures in the shear layer of the jet, frequency spectra were created by fourier transforms of the pixel intensity variation with time. The normalised pixel intensity values were used as the inputs to the fourier transforms. A high pass filter of 30Hz was applied to remove any low frequency noise due to the relatively short timespan of the recording sequences.

High Speed Photography, although capable of high frequency imaging of the entire jet flowfield, was not able to provide a quantitative measure of the amplitude of the coherent unsteadiness. Additionally, due to a lack of access, measurements inside the cooling hole tube were not possible with High Speed Photography. In contrast Hot Wire Anemometry (HWA) was capable of obtaining high frequency velocity measurements at sample rates in excess of 10kHz. The characteristics of HWA also meant that it was ideal for investigating the presence of coherent unsteady structures inside the cooling hole tube.

Single sensor hot wire probes, of type 55P01 from the Dantec Dynamics range, were used. The axis of the wire was perpendicular to the probe axis and supported by straight prongs. The hot wire itself was a platinum-plated tungsten wire of 15-20μm diameter and length 3mm. Gold plating at each end of the wire meant that the effective measurement length was 1.25mm. The overheat was set appropriately, and for a velocity of approximately $2ms^{-1}$ the step response was always less than 75μs, so implying that the maximum frequency response was 13kHz.

The hot wire probe was connected to a Dantec Dynamics 56 series CTA unit. The output from the wheatstone bridge was linearised and then low pass filtered to remove any high frequency aliasing. The low pass filter was a two-pole Butterworth filter with a cut-off frequency of 1kHz. The output from the low pass filter was sampled at 3.5kHz by a National Instrument USB data acquisition unit. The resolution of this configuration was less than $\pm 1 \times 10^{-5}$ms^{-1}.

The output from the low pass filter was sampled for 30s for each datapoint. This 30s sample was then split into thirty samples of 1s in length. Fourier transforms were performed on these shorter samples and the resulting spectra were averaged to give the overall frequency spectrum.

The removable module shown in Fig. 3 was modified to allow the hot wire probe to enter into the cooling hole tube. Within the cylindrical hole the hot wire could be located in one of three planes normal to the hole axis. These planes were located 0.5, 2 and 4.5D upstream of the hole exit centre. The hot wire was orientated with the wire axis perpendicular to the axial direction and with an angle of 20° to the blade spanwise direction. Measurements were taken with the mid point of the hot wire located on the hole centreline and 0.25D above and below the centreline. Geometric constraints meant that only the planes 2 and 4.5D upstream of the hole exit centre could be investigated for the fan-shaped hole.

The calibration curve for the hot wire in this configuration was found by plotting the average voltage at each blowing ratio with respect to the bulk velocity through the cooling hole. The assumption in this method of calibration was that the flow through the cooling hole was uniform. The High Speed Photography performed by Fawcett et al [12] suggested that the flow profile has some non-uniformity. In terms of the frequency spectra the uncertainty in the velocity amplitude is reduced to that of the hot wire voltage measurement, by scaling it with respect to the rms velocity.

Hot Wire Anemometry in the flowfield downstream of the cooling hole was performed on traverses normal to the blade surface 0D, 1D and 2D downstream of the hole exit centre. The distances quoted in the results section have their origin on the blade surface ignoring the geometry of the cooling holes. Hence, negative distances refer to measurements within the cooling hole.

In this second configuration the hot wire was calibrated before use independent of the Super Scale Cascade. The hot wire was located on the exit plane of a convergent nozzle. The dynamic pressure was found using the static pressure at the nozzle exit and the total pressure from a pitot probe upstream of the convergence. The mass flow rate through the nozzle was varied sinusoidally, through 6 cycles with a period of approximately 15s. The calibration curve for the hot wire was based on a velocity range of 2-6ms^{-1}.

Estimates of Uncertainty

The uncertainties in the experiment were calculated using the method described by Kline and McClintock [21]. The uncertainty in the CFR is less than 4%. Due to the method of finding the coolant mass flow rate the uncertainty in the blowing ratio increases with CFR. For a M of 1.0 this means that the uncertainty

Copyright © 2011 by Rolls-Royce plc

rises from 3% at a CFR of 0.1 up to 26% at a CFR of 0.8.

Aligning the hot wire manually meant that there was a positional uncertainty of ±1mm (0.08D) in the mainstream and ±0.5mm (0.04D) in the cooling hole tube.

The uncertainty in the Strouhal numbers presented in the results chapter are estimated at ±0.2 based on the uncertainty in the jet velocity and in identifying the dominant frequency.

RESULTS

Flowfield Downstream of the Cooling Hole

Time-Mean Effects In order to determine the impact of crossflow on the time-mean jet, images were recorded in the spanwise and secondary flow planes. The impact of crossflow upon the time-mean flow is seen most significantly in the secondary flow plane.

The time-mean flowfield in the secondary flow plane 2D downstream of the cylindrical hole is shown in Fig. 4, for blowing ratios (M) of 1.1 and 1.6 with a CFR of 0.1 to 0.6.

Figure 4 shows that varying the CFR causes the jet downstream to be rotationally displaced. This is illustrated by the rotation of the Counter Rotating Vortex Pair (CRVP). At a CFR of 0.1 the jet core is rotated in the clockwise direction (looking towards the hole exit) by approximately 20°, at a CFR of 0.2 the jet has no rotation, whilst a CFR of 0.6 causes the jet core to rotate anti-clockwise by 20°. Using a steady state computation Saumweber and Schulz [15] also show an anti-clockwise rotation of the CRVP, for M equal to 1.0 with a CFR of 1.0. Saumweber and Schultz suggested that this rotation increases the film effectiveness of the jet compared to the case with no crossflow.

Figure 5 shows the time mean jet from the fan-shaped hole in the same secondary flow plane as for the cylindrical hole in Fig. 4. The upper images of Fig. 5 show that at a CFR of 0.2 the flow has left the hole as a single jet attached to the blade surface. However, the lower half of Fig. 5 shows that at a CFR of 0.6 the flow exits the fan-shaped hole as two separate jets. The effectiveness results of Saumweber and Schulz [15] show the same splitting of the jet for a CFR of 0.7. Their measurements showed that this splitting gives a decrease in laterally averaged film effectiveness compared to the case with no crossflow.

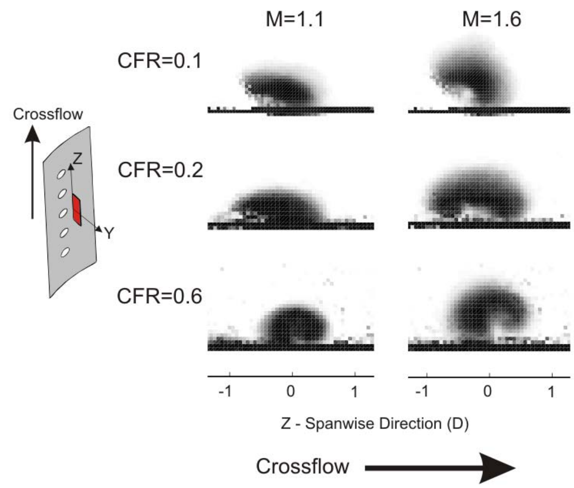

Figure 4. Time-mean images of the jet from a cylindrical hole seen in the secondary flow plane 2D downstream.

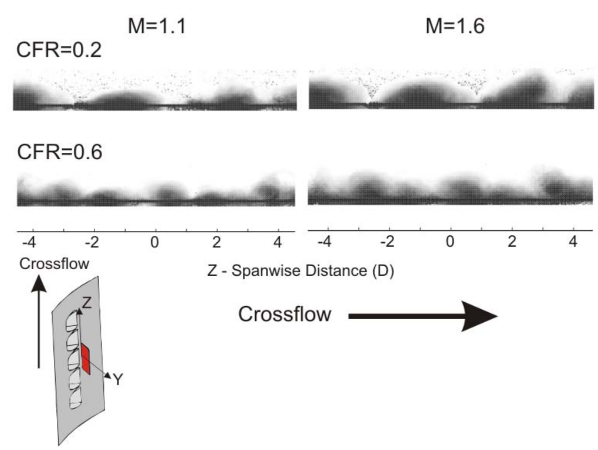

Figure 5. Time-mean images of the jet from a fan-shaped hole seen in the secondary flow plane 2D downstream.

Coherent Unsteady Structures Fawcett et al [12] showed experimentally that two coherent unsteady structures occur within the jet downstream of the hole exit, namely shear layer vortices and hairpin vortices. The influence of crossflow upon these is shown within this section.

Fawcett et al [12] discussed how the shear layer vortices were the result of a Kelvin-Helmholtz breakdown, with the velocity difference across the shear layer being the driving factor. The upper two images of Fig. 6 have a time period of 2ms between them, and show the passage of clockwise shear layer vortices in the jet from a cylindrical hole of M equal to 1.6 with a CFR of 0.1.

The lower image of Fig. 6 shows the local Strouhal numbers, obtained from fourier transforms based on the normalised pixel intensities. The coherence of the shear layer vortices is highlighted by the region in the shear layer with a consistent Strouhal number of 1.2. The Strouhal number, shown in Eq. 3, is based on

Copyright © 2011 by Rolls-Royce plc

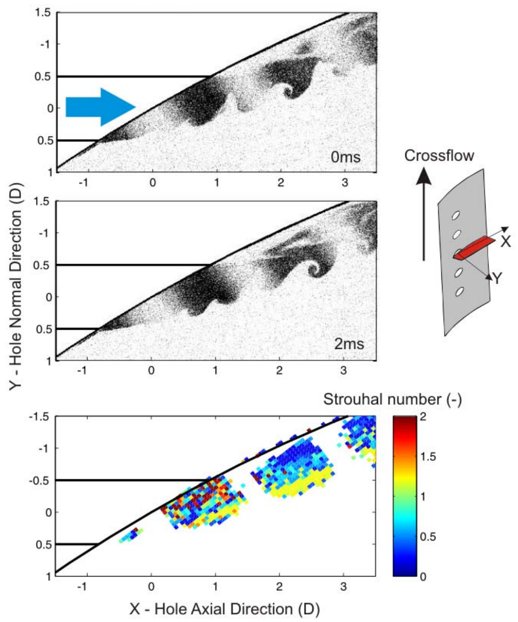

Figure 6. (Upper and centre) Shear layer vortices in the jet of M equal to 1.6 from a cylindrical hole with a CFR of 0.1. (Lower) The Strouhal number of coherent unsteadiness.

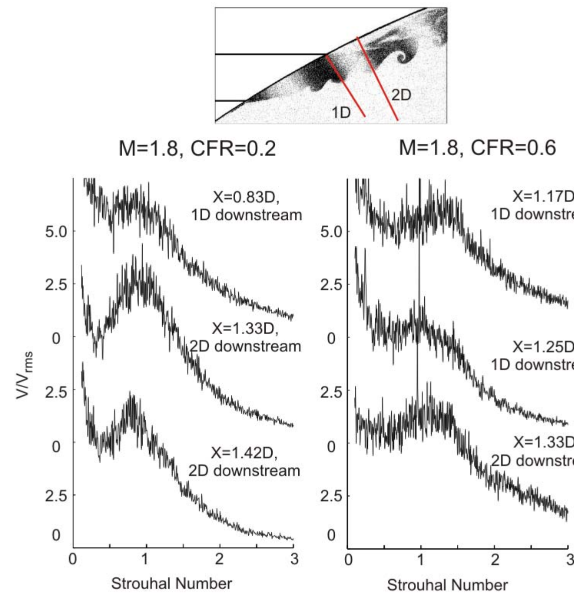

Figure 7. Frequency spectra within the shear layer of the jet from a cylindrical hole of M equal to 1.8 for CFR equal to 0.2 and 0.6.

the hole diameter and the local velocity of the structures. Measurements with Hot Wire Anemometry, within the jet shear layer 1D and 2D downstream of the hole exit, also show the presence of coherent unsteadiness with a Strouhal number of 1.0-1.2.

$$St = \frac{fD}{V_{local}} \tag{3}$$

Frequency spectra within the shear layer of the jet from the cylindrical hole of M equal to 1.8 with increasing crossflow velocity are shown in Fig. 7. The distances stated above the frequency spectra are those relative to the blade surface. The left side of Fig. 7 shows that coherent unsteadiness is present in the shear layer with a Strouhal number of 0.9 when the CFR is increased to 0.2. Although the Strouhal number of coherence is larger for the case at a higher CFR, shown on the right side of Fig. 7, the existence of a peak in the spectra suggests that the generation of shear layer vortices is unaffected by the increase in crossflow velocity.

The second type of coherent unsteady structures are the hairpin vortices and Fig. 8 shows their presence in the jet from a cylindrical hole of M equal to 0.7 and a CFR of 0.5. A schematic of the hairpin vortices is included in Fig. 8. The left hand side of Fig. 8 shows three images in the spanwise plane at intervals of 5ms, and from which the anti-clockwise vortex loops can be seen. The direction of rotation is opposite that of the shear layer vortices, as at this blowing ratio the velocity of the mainstream is greater than that of the jet.

The passing of a hairpin vortex in the secondary flow plane 2D downstream of the hole exit centre is shown on the right of Fig. 8. The image at 2ms shows the leading face of the vortex loop where the hairpin vortex is orientated in the spanwise direction. With increasing time the vorticity becomes orientated in the streamwise direction and passes through the measurement plane. 10ms after the hairpin vortex began to pass through the plane, the gap between the hairpin vortices is reached and the jet contracts back down onto the blade surface.

Similar observations on the image sequences obtained with High Speed Photography suggested that hairpin vortices are only present for low blowing ratios close to 0.7. The formation of hairpin vortices within the jet does not appear to be influenced by changing the CFR between 0.1 and 0.8.

Hairpin vortices are also present in the jet from a fan-shaped hole, as shown in Fig. 9 for M equal to 0.9 with a CFR of 0.1. The hairpin vortex shown in Fig. 9 has the same structure as that shown in Fig. 8 for the cylindrical jet. In the spanwise plane anti-clockwise vortex loops are seen, and in the secondary flow plane the passage of the leading face of the jet and the subsequent alignment of the vortex into the streamwise direction can be seen.

 Copyright © 2011 by Rolls-Royce plc

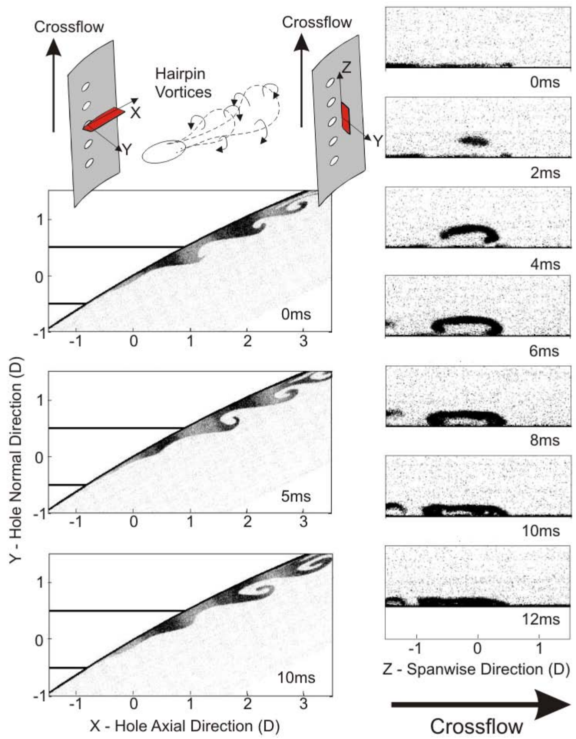

Figure 8. Hairpin vortices within the jet from a cylindrical hole of M equal to 0.7 with a CFR of 0.5 in the spanwise plane and secondary flow plane 2D downstream. Note the two sequences are not simultaneous.

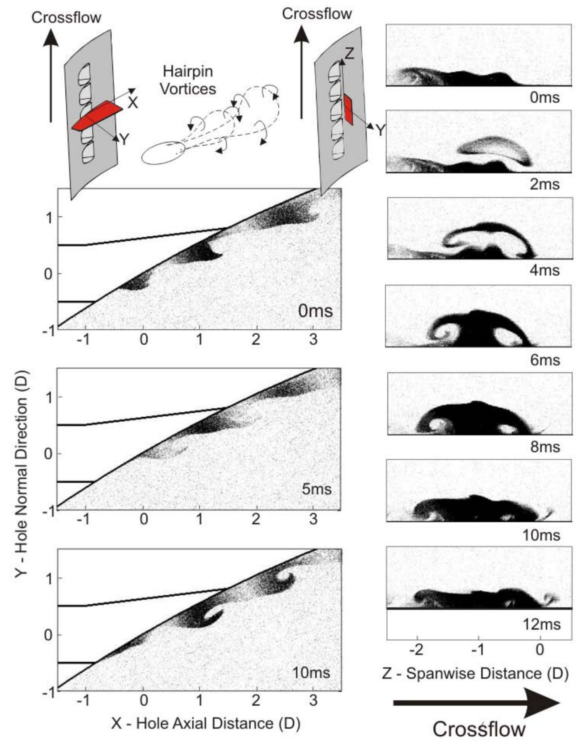

Figure 9. Hairpin vortices within the jet from a fan-shaped hole of M equal to 0.9 with a CFR of 0.1 in the spanwise plane and secondary flow plane 2D downstream. Note the two sequences are not simultaneous.

Hairpin vortices are present in the jet downstream of the fan-shaped hole for a M range of 0.7 through to 1.1. Like the cylindrical hole varying the CFR did not effect the presence of the hairpin vortices and they are present for a CFR range of up to 0.8. When the flow splits into two jets at higher CFR (as shown in Fig. 5), individual hairpin vortices form on both jets.

Fig. 10 shows that the hairpin vortices within the jet from the cylindrical hole at M equal to 0.7 and CFR equal to 0.5, from which the images in Fig. 8 where taken, are coherent and have a Strouhal number of 0.7. The images in Fig. 8 show that the hairpin vortices have a larger length scale relative to the jet thickness than the shear layer vortices shown in Fig. 6. Consequently the region of coherent unsteadiness shown in Fig. 10 encompasses the majority of the jet thickness.

Frequency spectra obtained with Hot Wire Anemometry within the jet core are also shown in Fig. 10. These frequency spectra show coherent unsteadiness of Strouhal number equal to 0.5 across a M range of 0.7 to 0.9 for a CFR of 0.1. The amplitude of the coherent unsteadiness ranges from 5% to 12% of the rms velocity. The value of the Strouhal number differs from that determined from the sequence of high speed images, however this can be attributed to the uncertainty in the local velocity measurement between the two techniques, and so it is believed that this coherent unsteadiness is also due to the passing of the hairpin vortices.

The contour plot of Figure 11 shows the Strouhal number in the spanwise plane across the sequence of images from which the images in Fig. 9 where taken. The hairpin vortices are seen to be coherent and have a Strouhal number of 0.6. As is seen to be the case for the cylindrical hole in Fig. 10 the coherent unsteadiness associated with the hairpin vortices extends across the majority of the jet thickness.

Frequency spectra obtained with Hot Wire Anemometry within the jet core are also shown in Fig. 11. Coherent unsteadiness with a Strouhal number of 0.4 is shown for M equal to 0.9 and 1.0 with a CFR of 0.1, and is suspected to be caused by the passage of the hairpin vortices.

The studies of Matsuda [10], Tyagi and Acharya [11] and

Copyright © 2011 by Rolls-Royce plc

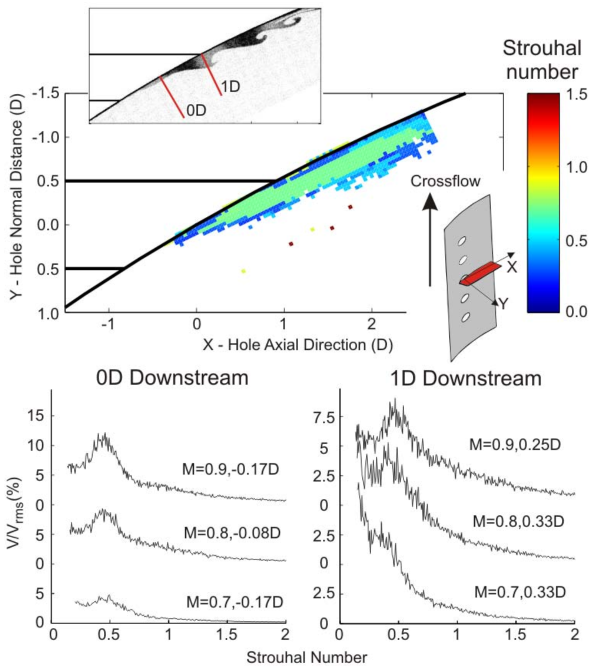

Figure 10. Strouhal number of the hairpin vortices seen with a cylindrical hole, (upper) for a jet of M equal to 0.7 and a CFR of 0.5 based on normalised pixel intensity and (lower) from velocity measurements in the shear layer of jets of M equal to 0.7 to 0.9 with a CFR of 0.1.

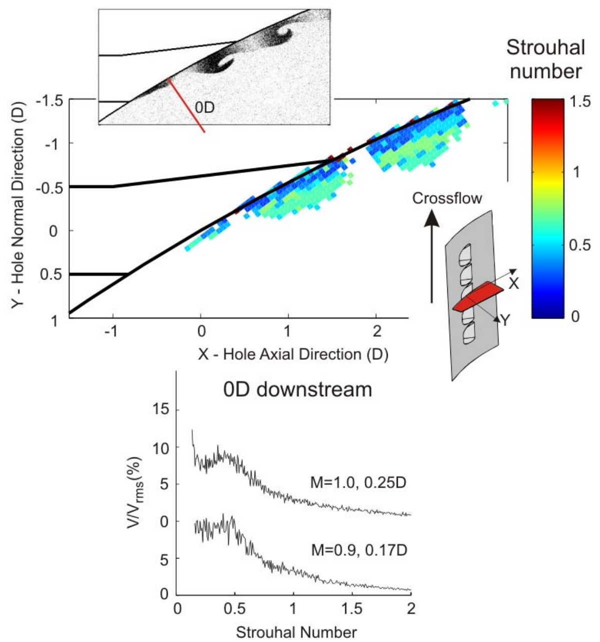

Figure 11. Strouhal number of the hairpin vortices seen with a fan-shaped hole, (upper) for a jet of M equal to 0.9 and a CFR of 0.1 based on normalised pixel intensity and (lower) from velocity measurements in the shear layer of jets of M equal to 0.9 to 1.0 with a CFR of 0.1.

Fawcett et al [12], in which hairpin vortices have been seen previously, did not have a crossflow at the hole inlet. This paper shows that crossflow has no impact upon the presence of hairpin vortices. Therefore it appears that the formation of hairpin vortices is independent of the flow condition at the hole inlet.

Considering this it is expected that hairpin vortices are the result of shear between the jet and the mainstream, as is the case for shear layer vortices. The hairpin shape is developed because at low blowing ratios the jet is attached to the blade surface downstream of the cooling hole. This means that the ends of the vortex are stretched on the underside of the jet closest to the blade surface. So hairpin vortices can be expected whenever there is a velocity difference in the shear layer of an attached jet.

The mixing between the jet and the mainstream will increase due to the presence of hairpin vortices. Depending on if this increase in mixing is in the lateral direction or in that normal to the blade surface, this could be either beneficial or detrimental to the film cooling effectiveness.

Coherent Unsteadiness Inside the Cooling Hole Tube

Frequency spectra obtained using Hot Wire Anemometry are shown in Fig. 12 for both cylindrical and fan-shaped holes on the hole axis 4.5D upstream of the hole exit centre. A blowing ratio range of 0.7 to 1.8 is shown with a CFR of 0.1.

Figure 12 shows that for both hole types there is coherent unsteadiness of approximately 210Hz at the highest blowing ratio of 1.8. As the blowing ratio is decreased the coherent unsteadiness at 210Hz is no longer present and instead coherent unsteadiness with a frequency of approximately 140Hz is observed at M equal to 1.0 and 1.2. At the lowest blowing ratios of 0.7 to 0.9 coherent unsteadiness at a frequency of approximately 70Hz is observed. The amplitude of the coherent unsteadiness shown in Fig. 12 is in the range of 3-10% of the rms velocity.

The coherent unsteadiness in Fig. 12 at 140Hz and 210Hz is suspected to be at a harmonic of the coherent unsteadiness at the fundamental harmonic of 70Hz. The three frequencies are therefore referred to within this section as the first, second and third harmonics. The Strouhal number of the first harmonic, based on the bulk jet velocity and the hole diameter, is in the range of 0.6-0.8.

Copyright © 2011 by Rolls-Royce plc

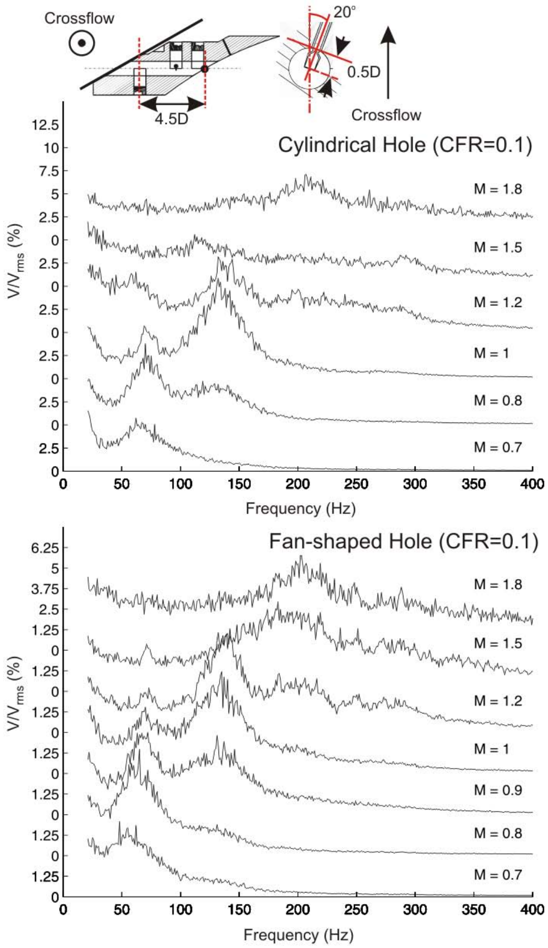

Figure 12. Frequency spectra on the hole centre line 4.5D upstream of the hole exit, for a CFR of 0.1. Note the vertical scales differ between the hole geometries.

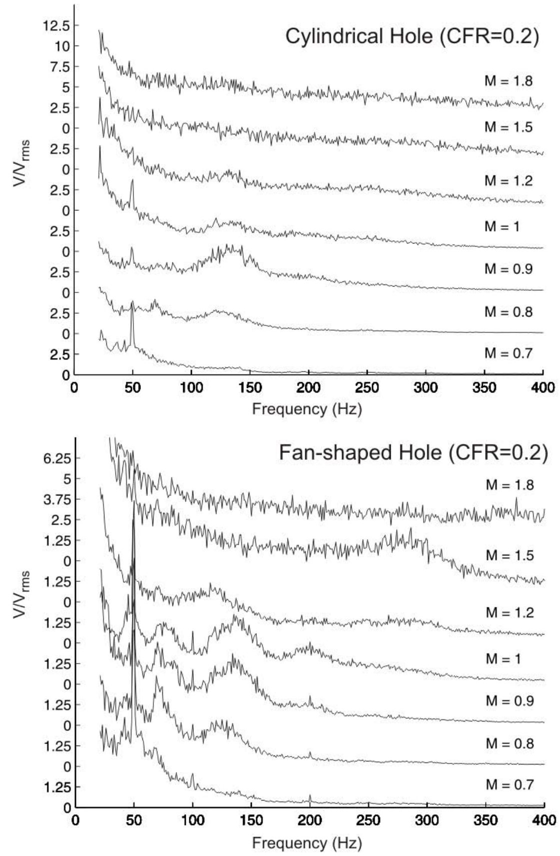

Figure 13. Frequency spectra on the hole centre line 4.5D upstream of the hole exit, for a CFR of 0.2. Note the vertical scales differ between the hole geometries.

The frequency spectra shown in Fig. 12 were repeatable, and were seen at the other measurement locations on the plane 4.5D upstream of the hole exit. Measurements on the plane 2D upstream of the hole exit for the cylindrical hole show only the presence of coherent unsteadiness at the two lowest harmonics. Measurements on the plane closest to the hole exit (0.5D upstream of the hole exit) show only the presence of the fundamental harmonic. Within the fan-shaped hole a similar decay in the higher order harmonics is seen, with only the fundamental harmonic present at the hole exit.

Figure 13 shows frequency spectra taken at the same measurement location as those in Fig. 12, but with an increase in the crossflow velocity to a CFR of 0.2. The peaks with a fundamental harmonic of 50Hz should be ignored in Fig. 13, as these are suspected to be caused by the blower at the end of the outlet pipe.

Figure 13 shows the coherent unsteadiness with a fundamental harmonic of 70Hz to be reduced in amplitude, for both hole geometries, compared to the spectra when the CFR is 0.1. Within the cylindrical hole coherent unsteadiness is only seen as a second order harmonic for M of 0.8 to 1.0, and as a first order harmonic at M equal to 0.8. Inside the fan-shaped hole coherent unsteadiness is seen at the first two harmonics across a M range of 0.8 to 1.0. Immediately upstream of the hole exit, as at a CFR of 0.1, only the fundamental harmonic is present.

Frequency spectra obtained with Hot Wire Anemometry within the cooling hole tube when the CFR is 0.6, are shown in Fig. 14 for the same measurement location as the lower CFRs shown in Figs. 12 and 13. The frequency spectra shown in Fig. 14

Copyright © 2011 by Rolls-Royce plc

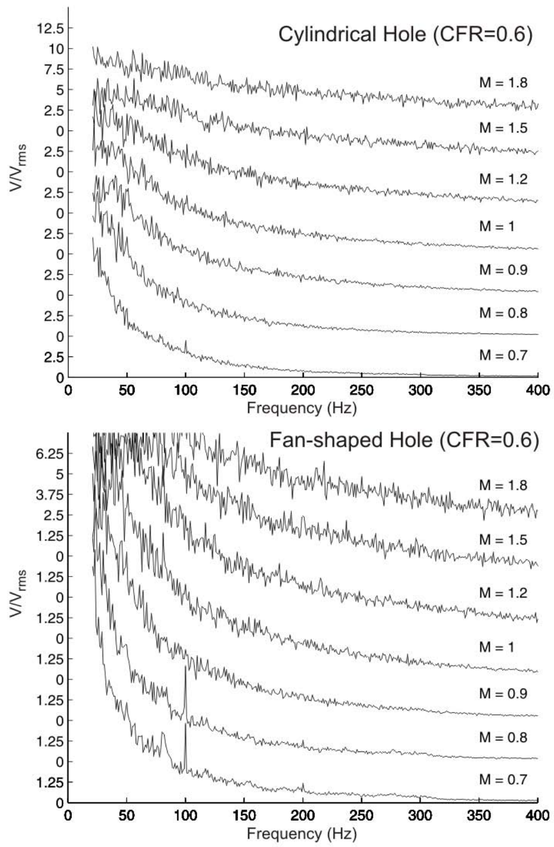

Figure 14. Frequency spectra on the hole centre line 4.5D upstream of the hole exit, for a CFR of 0.6. Note the vertical scales differ between the hole geometries.

do not show any coherent unsteadiness at any M, and further measurements at different upstream planes suggest this is the case all along the hole tube. Considering that there is also a reduction in the number of harmonics on increasing the CFR from 0.1 to 0.2, it appears that the presence of coherent unsteadiness inside the cooling hole reduces due to the increase in the crossflow velocity at the hole inlet.

Kiya and Sasaki [22] and Cherry et al [23] showed that coherent vortices are shed from a separation bubble on the leading edge of a flat plate. The cause of the coherent unsteadiness inside the hole is therefore suspected to be vortices shed from the separation bubble at the hole inlet. It is suspected the vortices are initially shed at the fundamental harmonic of 70Hz, and then decay with downstream distance to the higher order harmonics and eventually turbulence. The difference with change in blowing ratio, shown in Figs. 13 and 14, could possibly be explained by the reduction in the length of the separation bubble and the increase in the rms velocity with increasing blowing ratio.

Increasing the crossflow velocity to a CFR equal to 0.6, is suspected to bias the separation bubble at the hole inlet towards the approaching crossflow, compared to the case with a CFR equal to 0.1. It is possible that this change will reduce the magnitude of the coherent unsteadiness produced within the separation bubble at the hole inlet.

The fundamental harmonic within the cooling hole is of a similar Strouhal number as the hairpin vortices seen downstream of the hole exit. The presence of crossflow at the hole inlet does not impact on the formation of the hairpin vortices to the same extent that it does the in-hole coherent unsteadiness. However, the similarity in the Strouhal numbers suggests there may be a link between the two types of coherent unsteadiness.

CONCLUSIONS

The impact of spanwise crossflow upon cylindrical and fan-shaped film cooling holes located on a turbine blade pressure surface has been investigated experimentally. Attention has focused on the coherent unsteadiness arising within the jet and inside the cooling hole tube. Crossflow velocities of up to 0.8 times the bulk jet velocity have been studied for cooling holes of blowing ratios in the range of 0.7 to 1.8.

The time-mean flowfield downstream of the cooling hole, shows that a crossflow velocity of 0.6 times the bulk jet velocity causes the orientation of the jet from a cylindrical hole to twist by 20°. The same magnitude of crossflow also causes the jet from a fan-shaped hole to split in two within the diffusing exit of the hole.

Two coherent unsteady structures are seen in the jet downstream of the hole exit, namely hairpin vortices and shear layer vortices. Shear layer vortices with a Strouhal number of 1.0-1.2 occur in the shear layer of the separated jet from a cylindrical hole at higher blowing ratios. Hairpin vortices of a Strouhal number of approximately 0.5 are present in the attached jet downstream of both cylindrical and fan-shaped holes at blowing ratios of 0.7 to 0.9 and 0.7 to 1.1 respectively. The presence of both unsteady structures is not significantly affected by variations in the spanwise crossflow. Their persistence near the hole exit suggests that film cooling flows are strongly coherently unsteady, and so predictive methods based on steady-flows, such as RANS codes, are unlikely to capture near-hole film effectiveness correctly.

For the first time in-hole hot wire measurements have shown the presence of coherent unsteadiness within the cooling hole tube of both cylindrical and fan-shaped holes. Coherent unsteadiness, with a Strouhal number of 0.6 to 0.8, is seen at low crossflow velocities of up to 0.2 times the bulk jet velocity. The in-hole coherent unsteadiness, like the time-mean flowfield downstream of the hole exit, appears to be strongly dependent on the crossflow and is not observed at higher crossflow velocities. This

Copyright © 2011 by Rolls-Royce plc

suggests that should it be desired to minimise the in-hole coherent unsteadiness it may be possible to achieve this by altering the crossflow direction and magnitude.

ACKNOWLEDGMENT

This work has been funded by the EPSRC and Rolls-Royce plc. The authors would like to thank the EPSRC Engineering Instrument Loan Pool for the provision of the equipment for High Speed Photography.

REFERENCES

[1] Rolls-Royce., 2005. *The Jet Engine*, 5th ed. Rolls Royce Technical Publications.

[2] Goldstein, R., Eckert, E., and Burggraf, F., 1974. "Effects of hole geometry and density on three-dimesional film cooling". *International Journal of Heat and Mass Transfer,* ***17***(5), pp. 595–607.

[3] Sinha, A., Bogard, D., and Crawford, M., 1991. "Film-cooling effectiveness downstream of a single row of holes with variable density ratio". *Journal of Turbomachinery,* ***113***(3), pp. 442–449.

[4] Pietrzyk, J., Bogard, D., and Crawford, M., 1989. "Hydrodynamic measurements of jets in crossflow for gas turbine film cooling applications". *Journal of Turbomachinery,* ***111***(2), pp. 139–145.

[5] Thole, K., Gritsch, M., Schulz, A., and Wittig, S., 1998. "Flowfield measurements for film-cooling holes with expanded exits". *Journal of Turbomachinery,* ***120***(2), pp. 327–336.

[6] Andreopoulos, J., 1985. "On the structure of jets in a crossflow". *Journal of Fluid Mechanics,* ***157***, pp. 163–197.

[7] Fric, T., and Roshko, A., 1994. "Vortical structure in the wake of a transverse jet". *Journal of Fluid Mechanics,* ***279***, pp. 1–47.

[8] Kelso, R., Lim, T., and Perry, A., 1996. "An experimental study of round jets in cross-flow". *Journal of Fluid Mechanics,* ***306***, pp. 111–144.

[9] Lim, T., New, T., and Luo, S., 2001. "On the development of large-scale structures of a jet normal to a cross flow". *Physics of Fluids,* ***13***(3), pp. 770–775.

[10] Matsuda, H., Lida, S., and Hayakawa, M., 1990. "Coherent structures in a 3-dimensional wall jet". *Journal of Fluids Engineering,* ***112***, pp. 462–467.

[11] Tyagi, M., and Acharya, S., 2003. "Large eddy simulation of film cooling flow from an inclinded cylindrical jet". *Journal of Turbomachinery,* ***125***(4), pp. 734–742.

[12] Fawcett, R., Wheeler, A., He, L., and Taylor, R., 2010. "Experimental investigation into unsteady effects on film cooling". In Proceedings of the ASME Turbo Expo, Glasgow, GT2010-22603.

[13] Gritsch, M., Schulz, A., and Wittig, S., 1998. "Adiabatic wall effectiveness measurements of film-cooling holes with expanded exits". *Journal of Turbomachinery,* ***120***(3), pp. 549–556.

[14] Gritsch, M., Schulz, A., and Wittig, S., 2003. "Effect of internal coolant crossflow the effectiveness of shaped film-cooling holes". *Journal of Turbomachinery,* ***125***(3), pp. 547–554.

[15] Saumweber, C., and Schulz, A., 2008. "Comparison of the cooling performance of cylindrical and fan-shaped cooling holes with special emphasis on the effect of internal coolant crossflow". In Proceedings of the ASME Turbo Expo, Berlin, GT2008-51036.

[16] Peterson, S., and Plesniak, M., 2004. "Evolution of jets emanating from short holes into crossflow". *Journal of Fluid Mechanics,* ***503***, pp. 57–91.

[17] Thole, K., Gritsch, M., Schulz, A., and Wittig, S., 1997. "Effect of a crossflow at the entrance to a film cooling hole". *Journal of Fluids Engineering,* ***119***, pp. 533–540.

[18] Kholi, A., and Thole, K., 1997. "A CFD investigation on the effects of entrance crossflow directions to film cooling holes". In Proceedings of the ASME Heat Transfer Division, pp. 223–232.

[19] Palafox, P., 2006. "Gas turbine tip leakage flow and heat transfer". PhD Thesis, Department of Engineering Science University of Oxford.

[20] EN ISO 5167-2:2003. *Measurement of fluid flow by means of pressure differential devices inserted in circular-cross section conduits running full - Part 2: Orifice Plates.*

[21] Kline, S., and McClintock, F., 1953. "Describing uncertainties in single-sample experiments". *Mechanical Engineering*, January, pp. 3–8.

[22] Kiya, M., and Sasaki, K., 1983. "Structure of a turbulent separation bubble". *Journal of Fluid Mechanics,* ***137***, pp. 83–113.

[23] Cherry, N., Hillier, R., and Latour, M., 1984. "Unsteady measurements in a separated and reattaching flow". *Journal of Fluid Mechanics,* ***144***, pp. 13–46.

Copyright © 2011 by Rolls-Royce plc